



Observation of $\eta_c(2S) \rightarrow p\bar{p}$ and search for $X(3872) \rightarrow p\bar{p}$ decays



LHCb Collaboration

ARTICLE INFO

Article history:

Received 22 July 2016

Received in revised form 23 February 2017

Accepted 23 March 2017

Available online 28 March 2017

Editor: M. Doser

ABSTRACT

The first observation of the decay $\eta_c(2S) \rightarrow p\bar{p}$ is reported using proton–proton collision data corresponding to an integrated luminosity of 3.0 fb^{-1} recorded by the LHCb experiment at centre-of-mass energies of 7 and 8 TeV. The $\eta_c(2S)$ resonance is produced in the decay $B^+ \rightarrow [c\bar{c}]K^+$. The product of branching fractions normalised to that for the J/ψ intermediate state, $\mathcal{R}_{\eta_c(2S)}$, is measured to be

$$\mathcal{R}_{\eta_c(2S)} \equiv \frac{\mathcal{B}(B^+ \rightarrow \eta_c(2S)K^+) \times \mathcal{B}(\eta_c(2S) \rightarrow p\bar{p})}{\mathcal{B}(B^+ \rightarrow J/\psi K^+) \times \mathcal{B}(J/\psi \rightarrow p\bar{p})} = (1.58 \pm 0.33 \pm 0.09) \times 10^{-2},$$

where the first uncertainty is statistical and the second systematic. No signals for the decays $B^+ \rightarrow X(3872)(\rightarrow p\bar{p})K^+$ and $B^+ \rightarrow \psi(3770)(\rightarrow p\bar{p})K^+$ are seen, and the 95% confidence level upper limits on their relative branching ratios are found to be $\mathcal{R}_{X(3872)} < 0.25 \times 10^{-2}$ and $\mathcal{R}_{\psi(3770)} < 0.10$. In addition, the mass differences between the $\eta_c(1S)$ and the J/ψ states, between the $\eta_c(2S)$ and the $\psi(2S)$ states, and the natural width of the $\eta_c(1S)$ are measured as

$$M_{J/\psi} - M_{\eta_c(1S)} = 110.2 \pm 0.5 \pm 0.9 \text{ MeV},$$

$$M_{\psi(2S)} - M_{\eta_c(2S)} = 52.5 \pm 1.7 \pm 0.6 \text{ MeV},$$

$$\Gamma_{\eta_c(1S)} = 34.0 \pm 1.9 \pm 1.3 \text{ MeV}.$$

© 2017 Published by Elsevier B.V. This is an open access article under the CC BY license (<http://creativecommons.org/licenses/by/4.0/>). Funded by SCOAP³.

1. Introduction

Charmonium has proved to be a remarkable laboratory for the study of quantum chromodynamics in the non-perturbative regime. By comparing theoretical predictions with experimental results one can verify and tune the parameters of theoretical models in order to improve the accuracy of the predictions. In addition, in recent years, many exotic charmonium-like states have been observed, renewing interest in charmonium spectroscopy above the open-charm threshold [1,2]. The $B^+ \rightarrow p\bar{p}K^+$ decay¹ offers a clean environment to study intermediate resonances, such as charmonium and charmonium-like states decaying to $p\bar{p}$. The presence of $p\bar{p}$ in the final state allows intermediate states of any quantum number to be studied.

The first radial excitation $\eta_c(2S)$ of the charmonium ground state $\eta_c(1S)$ was observed at the B factories [3–5] and, to date,

only a few of its decay modes have been observed. LHCb has previously measured, using data corresponding to an integrated luminosity of 1 fb^{-1} , the decay $B^+ \rightarrow p\bar{p}K^+$ and the branching fractions of its intermediate charmonium contributions. Upper limits on the $\eta_c(2S)$, $X(3872)$ and $X(3915)$ branching fractions were also provided [6]. The BESIII Collaboration has also recently searched for the $\eta_c(2S) \rightarrow p\bar{p}$ decay in $\psi(2S)$ radiative transitions [7], and set an upper limit on the product of branching fractions $\mathcal{B}(\psi(3686) \rightarrow \eta_c(2S)\gamma) \times \mathcal{B}(\eta_c(2S) \rightarrow p\bar{p})$.

The $\eta_c(1S)$ state is the lowest-lying S-wave spin-singlet charmonium state and has been observed in various processes. The measurements of the $\eta_c(1S)$ mass and width in radiative charmonium transitions show a tension with those determined in different processes such as photon–photon fusion and B decays [8]. Detailed investigations of the line shape of the magnetic dipole transition by the KEDR [9] and CLEO [10] Collaborations indicate that additional factors modify the naïve k^3 dependence on the photon momentum, k , assumed in earlier measurements. This would affect the measurements of the mass and width in radiative charmonium transitions.

¹ The inclusion of charge-conjugate modes is implied throughout the paper.

In this paper, the first observation of $\eta_c(2S) \rightarrow p\bar{p}$ decay and a search for $\psi(3770) \rightarrow p\bar{p}$ and $X(3872) \rightarrow p\bar{p}$ decays are reported. The measurements of the branching fractions are relative to that of the $B^+ \rightarrow J/\psi(\rightarrow p\bar{p})K^+$ decay. Additional measurements of the $\eta_c(1S)$ and $\eta_c(2S)$ mass and the $\eta_c(1S)$ width are reported. This new measurement of the $\eta_c(1S)$ resonance parameters in exclusive $B^+ \rightarrow [c\bar{c}]K^+$ decays, where $[c\bar{c}]$ stands for a generic charmonium resonance, is independent of the above-mentioned line-shape complications.

2. Detector and simulation

The LHCb detector [11,12] is a single-arm forward spectrometer covering the pseudorapidity range $2 < \eta < 5$, designed for the study of particles containing b or c quarks. The detector includes a high-precision tracking system consisting of a silicon-strip vertex detector surrounding the pp interaction region, a large-area silicon-strip detector located upstream of a dipole magnet with a bending power of about 4 Tm, and three stations of silicon-strip detectors and straw drift tubes placed downstream of the magnet. The tracking system provides a measurement of momentum, p , of charged particles with a relative uncertainty that varies from 0.5% at low momentum² to 1.0% at 200 GeV. The minimum distance of a track to a primary vertex (PV), the impact parameter (IP), is measured with a resolution of $(15 + 29/p_T) \mu\text{m}$, where p_T is the component of the momentum transverse to the beam, in GeV. Different types of charged hadrons are distinguished using information from two ring-imaging Cherenkov detectors. The online event selection is performed by a trigger, which consists of a hardware stage, based on information from the calorimeter and muon systems, followed by a software stage, which applies full event reconstruction.

At the hardware trigger stage, events are required to have high transverse energy in the calorimeters. For hadrons, the transverse energy threshold is 3.5 GeV. The software trigger requires the presence of a two-, three- or four-track secondary vertex with significant displacement from the primary pp interaction vertices. At least one charged particle must have p_T larger than 1.7 GeV and be inconsistent with originating from a PV. A multivariate algorithm [13] is used for the identification of secondary vertices consistent with the decay of a b hadron.

Non-resonant $B^+ \rightarrow p\bar{p}K^+$ events are simulated, uniformly distributed in phase space, as well as resonant modes such as $B^+ \rightarrow \eta_c(2S)(\rightarrow p\bar{p})K^+$, $B^+ \rightarrow X(3872)(\rightarrow p\bar{p})K^+$, $B^+ \rightarrow \psi(2S)(\rightarrow p\bar{p})K^+$ and $B^+ \rightarrow J/\psi(\rightarrow p\bar{p})K^+$ to optimise the signal selection and to evaluate the ratio of the efficiencies for each considered channel with respect to the normalisation mode. In the simulation, pp collisions are generated using PYTHIA 8 [14] with a specific LHCb configuration [15]. Decays of hadronic particles are described by EVTGEN [16], in which final-state radiation is simulated using PHOTOS [17]. The interaction of the generated particles with the detector, and its response, are implemented using the GEANT4 toolkit [18] as described in Ref. [19].

3. Event selection

The selection of the B^+ candidates is done in two stages. First, a selection using loose criteria to reduce the background, is performed, followed by a multivariate selection. The three final-state charged particles are required to have a track-fit $\chi^2/\text{ndf} < 3$, where ndf is the number of degrees of freedom. They must also have $p > 1500$ MeV, $p_T > 100$ MeV, and $\chi_{\text{IP}}^2 > 1$ with respect to

any primary vertex in the event, where χ_{IP}^2 is defined as the difference in the vertex-fit χ^2 of a given PV reconstructed with and without the considered track. Moreover, the sum of the transverse momenta of the final-state particles is required to be greater than 4500 MeV and the sum of their momenta is required to be greater than 20 GeV. Particle identification (PID) requirements, based on the RICH detector information, are applied to p and \bar{p} candidates. The discriminating variables between different particle hypotheses (π, K, p) are the differences between log-likelihood values $\Delta \ln \mathcal{L}_{\alpha\beta}$ under particle hypotheses α and β , respectively. The p and \bar{p} candidates are required to have $\Delta \ln \mathcal{L}_{p\pi} > -5$. The reconstructed B^+ candidates are required to have an invariant mass in the range 5.08–5.48 GeV. The PV associated to each B^+ candidate is defined to be the one for which the B^+ candidate has the smallest χ_{IP}^2 . The B^+ candidate is required to have a vertex fit with a $\chi^2/\text{ndf} < 12$ and a flight distance greater than 3 mm, a χ^2 for the flight distance greater than 500, an $\chi_{\text{IP}}^2 < 10$ with respect to the associated PV and a $p_T > 1000$ MeV. The angle between the reconstructed momentum of the B^+ candidate and the B^+ flight direction (θ_{fl}) is required to be $\theta_{\text{fl}} > 0.632$ mrad. The reconstructed candidates that meet the above criteria are further filtered using a Boosted Decision Tree (BDT) algorithm [20,21]. The BDT is trained on a signal sample of simulated $B^+ \rightarrow p\bar{p}K^+$ decays and a background sample of data taken from the upper B^+ -mass sideband in the range 5.34–5.48 GeV. The upper sideband is exploited to avoid partially reconstructed background mainly due to $B^{(+,0)} \rightarrow p\bar{p}K^+\pi^{(0,-)}$ decays, where the pion is not correctly reconstructed, with reconstructed masses smaller than the measured B^+ mass. The variables used by the BDT to discriminate between signal and background candidates are: the p_T of each reconstructed track; the sum of the transverse momenta of the final-state particles; the sum of their χ_{IP}^2 with respect to the primary vertex; the IP of the final-state particle with the highest p_T , with respect to the primary vertex; the number of final state particles with $p_T > 900$ GeV/c; the maximum distance of closest approach between any two of the final-state particles from the B^+ decay; the IP of the B^+ candidate with respect to the primary vertex; the distance between primary and secondary vertices; $\cos \theta_{\text{fl}}$; the χ^2/ndf of the secondary vertex; a pointing variable defined as $\frac{P \sin \theta}{P \sin \theta + \sum_i p_{T,i}}$, where P is the total momentum of the three-particle final state, θ is the angle between the vector sum of the momenta of the final-state particles and the direction of the flight distance of the B^+ , with $\sum_i p_{T,i}$ the sum of the transverse momenta of the final-state particles; and the log likelihood difference for each daughter between the assumed PID hypothesis and the pion hypothesis. The selection criterion on the BDT response is chosen by maximising the significance of the $\chi_{c1} \rightarrow p\bar{p}$ signal yield in data. The number of events from this well-known transition provides a control sample comparable in size to that of the $\eta_c(2S)$. With this optimisation 90% of the $B^+ \rightarrow p\bar{p}K^+$ signal candidates are retained while reducing the combinatorial background level by 83%.

4. Invariant mass spectra and event yields

An extended unbinned maximum likelihood fit is performed to the $p\bar{p}K^+$ invariant mass distribution shown in Fig. 1. The shapes of the different contributions are determined from simulation. The signal peak is parameterised using an Apollonios probability density function (PDF) [22]. The yield, mean and resolution are allowed to vary freely in the fit, while the tail parameters are fixed to the values obtained from simulation. The combinatorial background component is parameterised by an exponential function. Partially reconstructed background is parameterised using an ARGUS PDF [23] convolved with a Gaussian resolution function.

² Natural units with $c = 1$ are used throughout the paper.

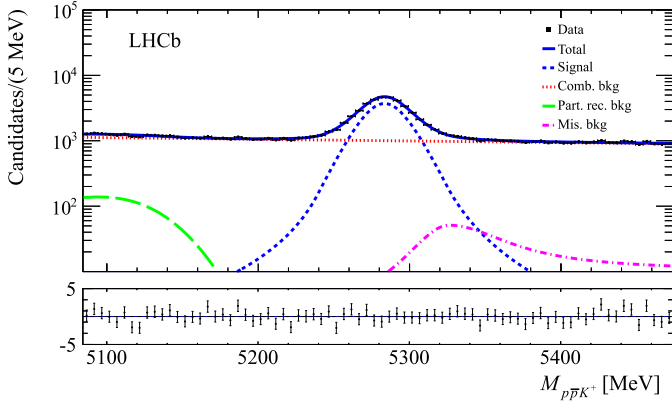


Fig. 1. Invariant mass spectrum of the $p\bar{p}K^+$ candidates. The total fit curve and individual fit components are superimposed on the data.

The parameters of the ARGUS PDF and of the Gaussian resolution function are fixed to the values obtained from simulation. The misidentified background due to $B^+ \rightarrow p\bar{p}\pi^+$ decays, where the charged pion is misidentified as a kaon, is parameterised with a bifurcated Gaussian PDF [24] and parameters fixed to the values obtained from simulation. The yields of partially reconstructed and misidentified backgrounds are determined from data.

The backgrounds observed in the $p\bar{p}K^+$ mass distribution are subtracted using the *sPlot* technique [25] to extract the $p\bar{p}$ mass spectrum in $B^+ \rightarrow p\bar{p}K^+$ decays. Signal yields for the resonant contributions are then determined from an extended unbinned maximum likelihood fit to the $p\bar{p}$ mass spectrum. To improve the $p\bar{p}$ invariant mass resolution, the fit to the B^+ decay vertex is performed with the B^+ mass constrained to the known value [8] and the B^+ candidate pointing to the PV [26]. The $p\bar{p}$ mass spectrum is also used to determine the mass differences $M_{J/\psi} - M_{\eta_c(1S)}$ and $M_{\psi(2S)} - M_{\eta_c(2S)}$ and the natural width of the $\eta_c(1S)$ state. In order to have accurate mass measurements, a calibration is applied to the momenta of the final-state particles. Large samples of $B^+ \rightarrow J/\psi K^+$ decays with $J/\psi \rightarrow \mu^+\mu^-$ are used to calibrate the momentum scale of the spectrometer [27]. Possible reflections due to $B^+ \rightarrow p\bar{\Lambda} \rightarrow p\bar{p}K^+$ decays are inves-

tigated using simulations, which show that no narrow structures are induced in the $p\bar{p}$ spectrum. Six charmonium resonances are included in the nominal fit to the $p\bar{p}$ invariant mass spectrum: $\eta_c(1S)$, J/ψ , χ_{c0} , χ_{c1} , $\eta_c(2S)$ and $\psi(2S)$. Alternative fits including the $\psi(3770)$ or the $X(3872)$ resonances are performed in order to estimate upper limits on their branching fractions. The J/ψ and $\psi(2S)$ peaks are parameterised with a double Gaussian PDF. The $\eta_c(1S)$, $\eta_c(2S)$, χ_{c0} and $\psi(3770)$ shapes are modelled with a relativistic Breit–Wigner PDF convolved with a Gaussian PDF. The $X(3872)$ and the χ_{c1} are described with a Gaussian PDF since their natural width is much smaller than mass resolution. Due to the B^+ mass constraint in the vertex fit, the $p\bar{p}$ mass resolution is effectively constant in the entire $p\bar{p}$ spectrum. The mass resolution parameter, common to all the charmonium states, is found to be $\sigma_{p\bar{p}} = (4.3 \pm 0.4)$ MeV, in good agreement with the simulations. The masses of the χ_{c0} , χ_{c1} , $X(3872)$, $\psi(3770)$ and $X(3915)$ states are fixed to the known values [8]. The J/ψ and $\psi(2S)$ peak positions ($M_{J/\psi}$ and $M_{\psi(2S)}$), the mass differences ($M_{J/\psi} - M_{\eta_c(1S)}$ and $M_{\psi(2S)} - M_{\eta_c(2S)}$), and the natural width of the $\eta_c(1S)$ state ($\Gamma_{\eta_c(1S)}$) are free parameters and are obtained from the fit to the data. A Gaussian constraint to the average value for the natural width of the $\eta_c(2S)$ is applied [8]. The $p\bar{p}$ non-resonant component is assumed to have no relative orbital angular momentum, $J=0$. The fit includes a possible interference effect between the $\eta_c(1S)$ state and the $J=0$ non-resonant component. The amplitude is given by $|A|^2 = |A_{\text{non-res}} + f e^{i\delta} A_{\eta_c(1S)}|^2$, where $A_{\text{non-res}}$ is the amplitude of the non-resonant component, $A_{\eta_c(1S)}$ is the amplitude of the $\eta_c(1S)$ state, δ is the phase difference and f a normalisation factor. The shape of the non-resonant component in the $p\bar{p}$ mass spectrum follows a phase-space distribution [8]. The fit result is shown in Fig. 2. A zoom of the fit result in the range 3.55–4.00 GeV is shown by the inset in Fig. 2.

Using Wilks' theorem [28], the statistical significance for the $\eta_c(2S)$ signal is computed from the change in the best fit likelihood when omitting the signal under scrutiny, $\sqrt{2 \ln(L_{S+B}/L_B)}$, where L_{S+B} and L_B are the likelihoods from the nominal fit and from the fit without the $\eta_c(2S)$ signal component, respectively. The statistical significance for the $\eta_c(2S)$ signal is found to be 6.4 standard deviations. No evidence for the $\psi(3770)$ and $X(3872)$ resonances is found. The signal yields are reported in Table 1.

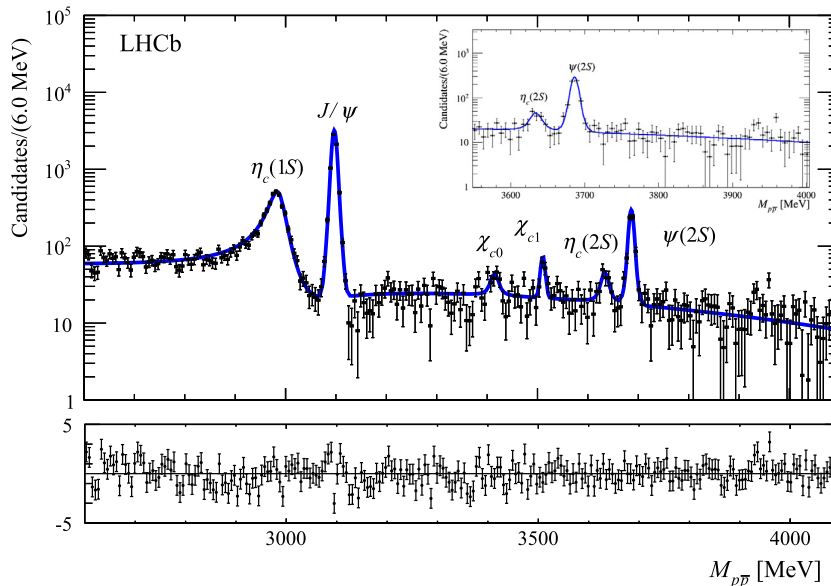


Fig. 2. Invariant mass spectrum of the $p\bar{p}$ candidates. Background in the $B^+ \rightarrow p\bar{p}K^+$ distribution is subtracted using the *sPlot* technique as described in the text. The total fit curve is superimposed. A zoom of the fit result in the range 3.55–4.00 GeV is shown by the inset.

Table 1

Signal yields from the fit to the $p\bar{p}$ mass spectrum in $B^+ \rightarrow p\bar{p}K^+$ decays. The fit fractions of the $\eta_c(1S)$ and the non-resonant component in the $J=0$ amplitude are 25% and 65% respectively. The fit fractions do not include uncertainties due to the ambiguities in the relative phase of the interfering amplitudes. Uncertainties are statistical only.

State	Signal yield
$\eta_c(1S)$ + non-res.	11246 ± 119
J/ψ	6721 ± 93
χ_{c0}	84 ± 22
χ_{c1}	95 ± 16
$\eta_c(2S)$	106 ± 22
$\psi(2S)$	588 ± 30
$\psi(3770)$	-6 ± 9
$X(3872)$	-14 ± 8

5. Efficiencies and systematic uncertainties

The branching fraction of the $B^+ \rightarrow [c\bar{c}](\rightarrow p\bar{p})K^+$ decay for a specific $[c\bar{c}]$ resonance relative to that of the J/ψ is given by

$$\begin{aligned} \mathcal{R}_{[c\bar{c}]} &\equiv \frac{\mathcal{B}(B^+ \rightarrow [c\bar{c}]K^+) \times \mathcal{B}([c\bar{c}] \rightarrow p\bar{p})}{\mathcal{B}(B^+ \rightarrow J/\psi K^+) \times \mathcal{B}(J/\psi \rightarrow p\bar{p})} \\ &= \frac{N([c\bar{c}])}{N(J/\psi)} \times \frac{\epsilon_{J/\psi}}{\epsilon_{c\bar{c}}}, \end{aligned} \quad (1)$$

where $N([c\bar{c}]) \equiv N(B^+ \rightarrow [c\bar{c}](\rightarrow p\bar{p})K^+)$ and $N(J/\psi) \equiv N(B^+ \rightarrow J/\psi(\rightarrow p\bar{p})K^+)$ are the numbers of decays and $\epsilon_{J/\psi}/\epsilon_{c\bar{c}}$ is the total efficiency ratio. The total efficiency is the product of the detector geometrical acceptance, the trigger efficiency, the reconstruction and selection efficiency, the PID efficiency, and the BDT classifier efficiency. The ratio of the efficiencies between the signal and the normalising J/ψ channels is determined using simulated samples. To account for any discrepancy between data and simulation, the PID efficiencies of kaons and protons are calibrated from data samples of $D^{*+} \rightarrow D^0(\rightarrow K^-\pi^+)\pi^+$ and $\Lambda^0 \rightarrow p\pi^-$ decays. For each simulated candidate, its PID value is replaced by a value extracted randomly from the corresponding PID curves determined from control samples. The selection is then applied to the PID-corrected simulated sample to estimate the efficiency.

Systematic uncertainties originate from the determination of the signal yields, efficiencies, selection procedure and branching fractions. Since the final state is common for all considered decays, most of the systematic uncertainties cancel in the ratios. Imperfect knowledge of the invariant mass distributions for the signal and background causes systematic uncertainties in the signal yield determination, the mass difference and width measurements. The contribution from the fit model is studied by using alternative shapes for the B^+ component, for the $[c\bar{c}]$ states and for the background. For the B^+ signal shape, a Gaussian PDF with power-law tails on both sides and the sum of two Gaussian PDFs with power-law tails are used as alternatives to the Apollonios PDF. The combinatorial background component in the $p\bar{p}K^+$ invariant mass is parameterised using a linear PDF. The effect of removing the peaking background due to misidentified $B^+ \rightarrow p\bar{p}\pi^+$ decays is investigated by checking the variation of the ratio of the branching fractions by including or neglecting this component in the fit. Incorrect modelling of the partially reconstructed background can also introduce a systematic uncertainty. This is estimated by removing the $p\bar{p}K^+$ invariant mass fit range below 5.20 GeV in order to exclude its contribution. In the fit to the $p\bar{p}$ spectrum, for the J/ψ signal, the Apollonios PDF is used as an alternative to the sum of two Gaussian PDFs. The range of the $p\bar{p}$ invariant mass spectrum is also varied. The systematic uncertainty due to the variation of the fit range gives a negligible contribution to the

Table 2

Systematic uncertainties in units of 10^{-4} on the $\eta_c(2S)$, $X(3872)$ and $\psi(3770)$ branching fraction measurements relative to that of the J/ψ . The efficiency contribution includes both the PID efficiency variation and the statistical error due to the finite size of the simulated samples.

	$\eta_c(2S)$	$X(3872)$	$\psi(3770)$
Fit	5	3	5
BDT	8	2	11
Efficiency	2	1	1
Total	9	4	12

Table 3

Systematic uncertainties on the mass differences $M_{J/\psi} - M_{\eta_c(1S)}$, $M_{\psi(2S)} - M_{\eta_c(2S)}$ and the $\Gamma_{\eta_c(1S)}$ measurements. The systematic uncertainty associated to the momentum scale calibration is negligible for the total width $\Gamma_{\eta_c(1S)}$ measurement.

	$M_{J/\psi} - M_{\eta_c(1S)}$ [MeV]	$M_{\psi(2S)} - M_{\eta_c(2S)}$ [MeV]	$\Gamma_{\eta_c(1S)}$ [MeV]
Fit	0.90	0.10	1.20
BDT	0.21	0.55	0.40
Momentum scale	0.03	0.06	–
Total	0.92	0.56	1.27

branching fraction measurement while it is the largest contribution to the $M_{J/\psi} - M_{\eta_c(1S)}$ difference. The largest variation in the ratio of the branching fractions due to the fit model is assigned as the corresponding systematic uncertainty.

Possible biases related to the signal selection criteria are investigated by varying the BDT requirement and by checking the effect on the branching fraction ratio and on the efficiency ratio, after accounting for statistical fluctuations. The maximum variation in the ratio of the yields or the maximum variation in the mass difference and width measurements are considered as an estimate of the corresponding source of systematic uncertainty. In addition, variations in the procedure used to determine the PID efficiency and the uncertainty due to the finite size of the simulated samples, lead to an uncertainty on the efficiency ratio in the branching fractions evaluation. The total systematic uncertainties on the relative branching fraction measurements, determined by adding the individual contributions in quadrature, are listed in Table 2.

The significance, including systematic uncertainties, of the signals is determined by convolving the profile likelihoods used in the yield determinations with a Gaussian with a width equal to the size of the systematic uncertainties that affect the yield. From the modified profile likelihood the significance of the $\eta_c(2S)$ signal is found to be 6.0 standard deviations. The upper limits at 90% and 95% confidence level on the $X(3872)$ and $\psi(3770)$ ratio of branching fractions are determined from integrating the profile likelihood functions including systematic uncertainty.

The measurements of the mass differences $M_{J/\psi} - M_{\eta_c(1S)}$ and $M_{\psi(2S)} - M_{\eta_c(2S)}$ and the natural width of the $\eta_c(1S)$ state are further affected by the uncertainty in the momentum scale calibration. This systematic uncertainty is small for the mass differences and negligible (< 0.003 MeV) for the natural width. Table 3 summarises the systematic uncertainties on the measurement of the $M_{J/\psi} - M_{\eta_c(1S)}$, $M_{\psi(2S)} - M_{\eta_c(2S)}$ mass differences and on the $\eta_c(1S)$ natural width.

6. Results and conclusions

A search for the $\eta_c(2S)$, $\psi(3770)$ and $X(3872)$ contributions in $B^+ \rightarrow p\bar{p}K^+$ decays is performed using data corresponding to an integrated luminosity of 3.0 fb^{-1} recorded at centre-of-mass energies of $\sqrt{s} = 7 \text{ TeV}$ and 8 TeV . The branching fractions are determined using the $B^+ \rightarrow J/\psi(\rightarrow p\bar{p})K^+$ decay as normalisation channel. The $\eta_c(2S) \rightarrow p\bar{p}$ decay is observed for the first time with

a total significance of 6.0 standard deviations. The relative branching fraction is measured to be

$$\mathcal{R}_{\eta_c(2S)} = (1.58 \pm 0.33 \pm 0.09) \times 10^{-2},$$

where the first uncertainty is statistical and the second systematic. For the $B^+ \rightarrow X(3872)(\rightarrow p\bar{p})K^+$ and the $B^+ \rightarrow \psi(3770)(\rightarrow p\bar{p})K^+$ decays, the upper limits at 90 (95)% confidence level are

$$\mathcal{R}_{\psi(3770)} < 9(10) \times 10^{-2},$$

$$\mathcal{R}_{X(3872)} < 0.20(0.25) \times 10^{-2}.$$

The visible branching fraction calculated using the value of $\mathcal{B}(B^+ \rightarrow J/\psi K^+) \times \mathcal{B}(J/\psi \rightarrow p\bar{p}) = (2.2 \pm 0.1) \times 10^{-6}$ [8] is determined to be

$$\begin{aligned} \mathcal{B}(B^+ \rightarrow \eta_c(2S)K^+) \times \mathcal{B}(\eta_c(2S) \rightarrow p\bar{p}) \\ = (3.47 \pm 0.72 \pm 0.20 \pm 0.16) \times 10^{-8}, \end{aligned}$$

where the last uncertainty is due to the uncertainty on $\mathcal{B}(B^+ \rightarrow J/\psi K^+) \times \mathcal{B}(J/\psi \rightarrow p\bar{p})$.

The differences between $M_{J/\psi}$ and $M_{\eta_c(1S)}$ and between $M_{\psi(2S)}$ and $M_{\eta_c(2S)}$ are measured to be

$$M_{J/\psi} - M_{\eta_c(1S)} = 110.2 \pm 0.5 \pm 0.9 \text{ MeV},$$

$$M_{\psi(2S)} - M_{\eta_c(2S)} = 52.5 \pm 1.7 \pm 0.6 \text{ MeV}.$$

The natural width of the $\eta_c(1S)$ is found to be

$$\Gamma_{\eta_c(1S)} = 34.0 \pm 1.9 \pm 1.3 \text{ MeV}.$$

In contrast to the determinations using radiative decays, these mass and width determinations do not depend on the knowledge of the line shapes of the magnetic dipole transition.

Acknowledgements

We express our gratitude to our colleagues in the CERN accelerator departments for the excellent performance of the LHC. We thank the technical and administrative staff at the LHCb institutes. We acknowledge support from CERN and from the national agencies: CAPES, CNPq, FAPERJ and FINEP (Brazil); NSFC (China); CNRS/IN2P3 (France); BMBF, DFG and MPG (Germany); INFN (Italy); FOM and NWO (The Netherlands); MNiSW and NCN (Poland); MEN/IFA (Romania); MinES and FANO (Russia); MinECo (Spain); SNSF and SER (Switzerland); NASU (Ukraine); STFC (United Kingdom); NSF (USA). We acknowledge the computing resources that are provided by CERN, IN2P3 (France), KIT and DESY (Germany), INFN (Italy), SURF (The Netherlands), PIC (Spain), GridPP (United Kingdom), RRCKI and Yandex LLC (Russia), CSCS (Switzerland), IFIN-HH (Romania), CBPF (Brazil), PL-GRID (Poland) and OSC (USA). We are indebted to the communities behind the multiple open source software packages on which we depend. Individual groups or members have received support from AvH Foundation (Germany), EPLANET, Marie Skłodowska-Curie Actions and ERC (European Union), Conseil Général de Haute-Savoie, Labex ENIGMASS and OCEVU, Région Auvergne (France), RFBR and Yandex LLC (Russia), GVA, XuntaGal and GENCAT (Spain), Herchel Smith Fund, The Royal Society, Royal Commission for the Exhibition of 1851 and the Leverhulme Trust (United Kingdom).

LHCb Collaboration

R. Aaij³⁹, B. Adeva³⁸, M. Adinolfi⁴⁷, Z. Ajaltouni⁵, S. Akar⁶, J. Albrecht¹⁰, F. Alessio³⁹, M. Alexander⁵², S. Ali⁴², G. Alkhazov³¹, P. Alvarez Cartelle⁵⁴, A.A. Alves Jr.⁵⁸, S. Amato², S. Amerio²³, Y. Amhis⁷,

References

- [1] N. Brambilla, et al., Heavy quarkonium: progress, puzzles, and opportunities, *Eur. Phys. J. C* 71 (2011) 1534, arXiv:1010.5827.
- [2] Particle Data Group, K.A. Olive, et al., Review of particle properties, Developments in heavy quarkonium spectroscopy (pages 1240–1247), *Chin. Phys. C* 38 (2014) 090001.
- [3] Belle Collaboration, S.K. Choi, et al., Observation of the $\eta_c(2S)$ in exclusive $B \rightarrow K K_S K^- \pi^+$ decays, *Phys. Rev. Lett.* 89 (2002) 102001, arXiv:hep-ex/0206002; Belle Collaboration, S.K. Choi, et al., *Phys. Rev. Lett.* 89 (2002) 129901 (Erratum).
- [4] BaBar Collaboration, B. Aubert, et al., Measurements of the mass and width of the η_c meson and of an $\eta_c(2S)$ candidate, *Phys. Rev. Lett.* 92 (2004) 142002, arXiv:hep-ex/0311038.
- [5] CLEO Collaboration, D.M. Asner, et al., Observation of η_c' production in $\gamma\gamma$ fusion at CLEO, *Phys. Rev. Lett.* 92 (2004) 142001, arXiv:hep-ex/0312058.
- [6] LHCb Collaboration, R. Aaij, et al., Measurements of the branching fractions of $B^+ \rightarrow p\bar{p}K^+$ decays, *Eur. Phys. J. C* 73 (6) (2013) 2462, arXiv:1303.7133.
- [7] BESIII Collaboration, M. Ablikim, et al., Search for $\eta_c(2S)/h_c \rightarrow p\bar{p}$ decays and measurements of the $\chi_{cJ} \rightarrow p\bar{p}$ branching fractions, *Phys. Rev. D* 88 (2013) 112001, arXiv:1310.6099.
- [8] Particle Data Group, K.A. Olive, et al., Review of particle physics, *Chin. Phys. C* 38 (2014) 090001, and 2015 update.
- [9] V.V. Anashin, et al., Measurement of $J/\psi \rightarrow \gamma\eta_c$ decay rate and η_c parameters at KEDR, *Phys. Lett. B* 738 (2014) 391, arXiv:1406.7644.
- [10] CLEO Collaboration, R.E. Mitchell, et al., J/ψ and $\psi(2S)$ radiative decays to η_c , *Phys. Rev. Lett.* 102 (2009) 011801, arXiv:0805.0252; CLEO Collaboration, R.E. Mitchell, et al., *Phys. Rev. Lett.* 106 (2011) 159903 (Erratum).
- [11] LHCb Collaboration, A.A. Alves Jr., et al., The LHCb detector at the LHC, *J. Instrum.* 3 (2008) S08005.
- [12] LHCb Collaboration, R. Aaij, et al., LHCb detector performance, *Int. J. Mod. Phys. A* 30 (2015) 1530022, arXiv:1412.6352.
- [13] V.V. Gligorov, M. Williams, Efficient, reliable and fast high-level triggering using a bonsai boosted decision tree, *J. Instrum.* 8 (2013) P02013, arXiv:1210.6861.
- [14] T. Sjöstrand, S. Mrenna, P. Skands, A brief introduction to PYTHIA 8.1, *Comput. Phys. Commun.* 178 (2008) 852, arXiv:0710.3820; T. Sjöstrand, S. Mrenna, P. Skands, PYTHIA 6.4 physics and manual, *J. High Energy Phys.* 05 (2006) 026, arXiv:hep-ph/0603175.
- [15] I. Belyaev, et al., Handling of the generation of primary events in Gauss, the LHCb simulation framework, *J. Phys. Conf. Ser.* 331 (2011) 032047.
- [16] D.J. Lange, The EvtGen particle decay simulation package, *Nucl. Instrum. Methods A* 462 (2001) 152.
- [17] P. Golonka, Z. Was, PHOTOS Monte Carlo: a precision tool for QED corrections in Z and W decays, *Eur. Phys. J. C* 45 (2006) 97, arXiv:hep-ph/0506026.
- [18] Geant4 Collaboration, J. Allison, et al., Geant4 developments and applications, *IEEE Trans. Nucl. Sci.* 53 (2006) 270; Geant4 Collaboration, S. Agostinelli, et al., Geant4: a simulation toolkit, *Nucl. Instrum. Methods A* 506 (2003) 250.
- [19] M. Clemencic, et al., The LHCb simulation application, Gauss: design, evolution and experience, *J. Phys. Conf. Ser.* 331 (2011) 032023.
- [20] L. Breiman, J.H. Friedman, R.A. Olshen, C.J. Stone, Classification and Regression Trees, Wadsworth International Group, Belmont, California, USA, 1984.
- [21] B.P. Roe, et al., Boosted decision trees as an alternative to artificial neural networks for particle identification, *Nucl. Instrum. Methods A* 543 (2005) 577, arXiv:physics/0408124.
- [22] D. Martínez Santos, F. Dupertuis, Mass distributions marginalized over percent errors, *Nucl. Instrum. Methods A* 764 (2014) 150, arXiv:1312.5000.
- [23] ARGUS Collaboration, H. Albrecht, et al., Measurement of the polarization in the decay $B \rightarrow J/\psi K^*$, *Phys. Lett. B* 340 (1994) 217.
- [24] BaBar Collaboration, P. del Amo Sanchez, et al., Study of $B \rightarrow X\gamma$ decays and determination of $|V_{td}/V_{ts}|$, *Phys. Rev. D* 82 (2010) 051101, arXiv:1005.4087.
- [25] M. Pivk, F. Le Diberder, sPlot: a statistical tool to unfold data distributions, *Nucl. Instrum. Methods A* 555 (2005) 356, arXiv:physics/0402083.
- [26] W.D. Hulsbergen, Decay chain fitting with a Kalman filter, *Nucl. Instrum. Methods A* 552 (2005) 566, arXiv:physics/0503191.
- [27] LHCb Collaboration, R. Aaij, et al., Measurements of the Λ_b^0 , Ξ_b^- , and Ω_b^- baryon masses, *Phys. Rev. Lett.* 110 (2013) 182001, arXiv:1302.1072.
- [28] S.S. Wilks, The large-sample distribution of the likelihood ratio for testing composite hypotheses, *Ann. Math. Stat.* 9 (1938) 60.

L. An⁴⁰, L. Anderlini¹⁸, G. Andreassi⁴⁰, M. Andreotti^{17,g}, J.E. Andrews⁵⁹, R.B. Appleby⁵⁵,
 O. Aquines Gutierrez¹¹, F. Archilli¹, P. d'Argent¹², J. Arnau Romeu⁶, A. Artamonov³⁶, M. Artuso⁶⁰,
 E. Aslanides⁶, G. Auriemma²⁶, M. Baalouch⁵, I. Babuschkin⁵⁵, S. Bachmann¹², J.J. Back⁴⁹, A. Badalov³⁷,
 C. Baesso⁶¹, W. Baldini¹⁷, R.J. Barlow⁵⁵, C. Barschel³⁹, S. Barsuk⁷, W. Barter³⁹, V. Batozskaya²⁹,
 B. Batsukh⁶⁰, V. Battista⁴⁰, A. Bay⁴⁰, L. Beaucourt⁴, J. Beddow⁵², F. Bedeschi²⁴, I. Bediaga¹, L.J. Bel⁴²,
 V. Bellee⁴⁰, N. Belloli^{21,i}, K. Belous³⁶, I. Belyaev³², E. Ben-Haim⁸, G. Bencivenni¹⁹, S. Benson³⁹,
 J. Benton⁴⁷, A. Berezhnoy³³, R. Bernet⁴¹, A. Bertolin²³, F. Betti¹⁵, M.-O. Bettler³⁹, M. van Beuzekom⁴²,
 S. Bifani⁴⁶, P. Billoir⁸, T. Bird⁵⁵, A. Birnkrant¹⁰, A. Bitadze⁵⁵, A. Bizzeti^{18,u}, T. Blake⁴⁹, F. Blanc⁴⁰,
 J. Blouw¹¹, S. Blusk⁶⁰, V. Bocci²⁶, T. Boettcher⁵⁷, A. Bondar³⁵, N. Bondar^{31,39}, W. Bonivento¹⁶,
 A. Borgheresi^{21,i}, S. Borghi⁵⁵, M. Borisyak⁶⁷, M. Borsato³⁸, F. Bossu⁷, M. Boubdir⁹, T.J.V. Bowcock⁵³,
 E. Bowen⁴¹, C. Bozzi^{17,39}, S. Braun¹², M. Britsch¹², T. Britton⁶⁰, J. Brodzicka⁵⁵, E. Buchanan⁴⁷,
 C. Burr⁵⁵, A. Bursche², J. Buytaert³⁹, S. Cadeddu¹⁶, R. Calabrese^{17,g}, M. Calvi^{21,i}, M. Calvo Gomez^{37,m},
 P. Campana¹⁹, D. Campora Perez³⁹, L. Capriotti⁵⁵, A. Carbone^{15,e}, G. Carboni^{25,j}, R. Cardinale^{20,*,h},
 A. Cardini¹⁶, P. Carniti^{21,i}, L. Carson⁵¹, K. Carvalho Akiba², G. Casse⁵³, L. Cassina^{21,i},
 L. Castillo Garcia⁴⁰, M. Cattaneo³⁹, Ch. Cauet¹⁰, G. Cavallero²⁰, R. Cenci^{24,t}, M. Charles⁸,
 Ph. Charpentier³⁹, G. Chatzikonstantinidis⁴⁶, M. Chefdeville⁴, S. Chen⁵⁵, S.-F. Cheung⁵⁶,
 V. Chobanova³⁸, M. Chruszcz^{41,27}, X. Cid Vidal³⁸, G. Ciezarek⁴², P.E.L. Clarke⁵¹, M. Clemencic³⁹,
 H.V. Cliff⁴⁸, J. Closier³⁹, V. Coco⁵⁸, J. Cogan⁶, E. Cogneras⁵, V. Cogoni^{16,39,f}, L. Cojocariu³⁰,
 G. Collazuol^{23,o}, P. Collins³⁹, A. Comerma-Montells¹², A. Contu³⁹, A. Cook⁴⁷, S. Coquereau⁸, G. Corti³⁹,
 M. Corvo^{17,g}, C.M. Costa Sobral⁴⁹, B. Couturier³⁹, G.A. Cowan⁵¹, D.C. Craik⁵¹, A. Crocombe⁴⁹,
 M. Cruz Torres⁶¹, S. Cunliffe⁵⁴, R. Currie⁵⁴, C. D'Ambrosio³⁹, E. Dall'Occo⁴², J. Dalseno⁴⁷, P.N.Y. David⁴²,
 A. Davis⁵⁸, O. De Aguiar Francisco², K. De Bruyn⁶, S. De Capua⁵⁵, M. De Cian¹², J.M. De Miranda¹,
 L. De Paula², P. De Simone¹⁹, C.-T. Dean⁵², D. Decamp⁴, M. Deckenhoff¹⁰, L. Del Buono⁸,
 M. Demmer¹⁰, D. Derkach⁶⁷, O. Deschamps⁵, F. Dettori³⁹, B. Dey²², A. Di Canto³⁹, H. Dijkstra³⁹,
 F. Dordei³⁹, M. Dorigo⁴⁰, A. Dosil Suárez³⁸, A. Dovbnya⁴⁴, K. Dreimanis⁵³, L. Dufour⁴², G. Dujany⁵⁵,
 K. Dungs³⁹, P. Durante³⁹, R. Dzhelyadin³⁶, A. Dziurda³⁹, A. Dzyuba³¹, N. Déleage⁴, S. Easo⁵⁰,
 U. Egede⁵⁴, V. Egorychev³², S. Eidelman³⁵, S. Eisenhardt⁵¹, U. Eitschberger¹⁰, R. Ekelhof¹⁰, L. Eklund⁵²,
 Ch. Elsasser⁴¹, S. Ely⁶⁰, S. Esen¹², H.M. Evans⁴⁸, T. Evans⁵⁶, A. Falabella¹⁵, N. Farley⁴⁶, S. Farry⁵³,
 R. Fay⁵³, D. Fazzini^{21,i}, D. Ferguson⁵¹, V. Fernandez Albor³⁸, F. Ferrari^{15,39}, F. Ferreira Rodrigues¹,
 M. Ferro-Luzzi³⁹, S. Filippov³⁴, M. Fiore^{17,g}, M. Fiorini^{17,g}, M. Firlej²⁸, C. Fitzpatrick⁴⁰, T. Fiutowski²⁸,
 F. Fleuret^{7,b}, K. Fohl³⁹, M. Fontana¹⁶, F. Fontanelli^{20,h}, D.C. Forshaw⁶⁰, R. Forty³⁹, V. Franco Lima⁵³,
 M. Frank³⁹, C. Frei³⁹, J. Fu^{22,q}, E. Furfaro^{25,j}, C. Färber³⁹, A. Gallas Torreira³⁸, D. Galli^{15,e}, S. Gallorini²³,
 S. Gambetta⁵¹, M. Gandelman², P. Gandini⁵⁶, Y. Gao³, J. García Pardiñas³⁸, J. Garra Tico⁴⁸, L. Garrido³⁷,
 P.J. Garsed⁴⁸, D. Gascon³⁷, C. Gaspar³⁹, L. Gavardi¹⁰, G. Gazzoni⁵, D. Gerick¹², E. Gersabeck¹²,
 M. Gersabeck⁵⁵, T. Gershon⁴⁹, Ph. Ghez⁴, S. Gianì⁴⁰, V. Gibson⁴⁸, O.G. Girard⁴⁰, L. Giubega³⁰,
 K. Gizdov⁵¹, V.V. Gligorov⁸, D. Golubkov³², A. Golutvin^{54,39}, A. Gomes^{1,a}, I.V. Gorelov³³, C. Gotti^{21,i},
 M. Grabalosa Gándara⁵, R. Graciani Diaz³⁷, L.A. Granado Cardoso³⁹, E. Graugés³⁷, E. Graverini⁴¹,
 G. Graziani¹⁸, A. Grecu³⁰, P. Griffith⁴⁶, L. Grillo²¹, B.R. Gruberg Cazon⁵⁶, O. Grünberg⁶⁵, E. Gushchin³⁴,
 Yu. Guz³⁶, T. Gys³⁹, C. Göbel⁶¹, T. Hadavizadeh⁵⁶, C. Hadjivasiliou⁵, G. Haefeli⁴⁰, C. Haen³⁹,
 S.C. Haines⁴⁸, S. Hall⁵⁴, B. Hamilton⁵⁹, X. Han¹², S. Hansmann-Menzemer¹², N. Harnew⁵⁶,
 S.T. Harnew⁴⁷, J. Harrison⁵⁵, M. Hatch³⁹, J. He⁶², T. Head⁴⁰, A. Heister⁹, K. Hennessy⁵³, P. Henrard⁵,
 L. Henry⁸, J.A. Hernando Morata³⁸, E. van Herwijnen³⁹, M. Heß⁶⁵, A. Hicheur², D. Hill⁵⁶,
 C. Hombach⁵⁵, W. Hulsbergen⁴², T. Humair⁵⁴, M. Hushchyn⁶⁷, N. Hussain⁵⁶, D. Hutchcroft⁵³,
 M. Idzik²⁸, P. Ilten⁵⁷, R. Jacobsson³⁹, A. Jaeger¹², J. Jalocha⁵⁶, E. Jans⁴², A. Jawahery⁵⁹, M. John⁵⁶,
 D. Johnson³⁹, C.R. Jones⁴⁸, C. Joram³⁹, B. Jost³⁹, N. Jurik⁶⁰, S. Kandybei⁴⁴, W. Kanso⁶, M. Karacson³⁹,
 J.M. Kariuki⁴⁷, S. Karodia⁵², M. Kecke¹², M. Kelsey⁶⁰, I.R. Kenyon⁴⁶, M. Kenzie³⁹, T. Ketel⁴³,
 E. Khairullin⁶⁷, B. Khanji^{21,39,i}, C. Khurewathanakul⁴⁰, T. Kirn⁹, S. Klaver⁵⁵, K. Klimaszewski²⁹,
 S. Koliiev⁴⁵, M. Kolpin¹², I. Komarov⁴⁰, R.F. Koopman⁴³, P. Koppenburg⁴², A. Kozachuk³³, M. Kozeiha⁵,
 L. Kravchuk³⁴, K. Kreplin¹², M. Kreps⁴⁹, P. Krokovny³⁵, F. Kruse¹⁰, W. Krzemien²⁹, W. Kucewicz^{27,l},
 M. Kucharczyk²⁷, V. Kudryavtsev³⁵, A.K. Kuonen⁴⁰, K. Kurek²⁹, T. Kvaratskheliya^{32,39}, D. Lacarrere³⁹,
 G. Lafferty^{55,39}, A. Lai¹⁶, D. Lambert⁵¹, G. Lanfranchi¹⁹, C. Langenbruch⁹, B. Langhans³⁹, T. Latham⁴⁹,
 C. Lazzeroni⁴⁶, R. Le Gac⁶, J. van Leerdam⁴², J.-P. Lees⁴, A. Leflat^{33,39}, J. Lefrançois⁷, R. Lefèvre⁵,

F. Lemaître³⁹, E. Lemos Cid³⁸, O. Leroy⁶, T. Lesiak²⁷, B. Leverington¹², Y. Li⁷, T. Likhomanenko^{67,66}, R. Lindner³⁹, C. Linn³⁹, F. Lionetto⁴¹, B. Liu¹⁶, X. Liu³, D. Loh⁴⁹, I. Longstaff⁵², J.H. Lopes², D. Lucchesi^{23,0}, M. Lucio Martinez³⁸, H. Luo⁵¹, A. Lupato²³, E. Luppi^{17,g}, O. Lupton⁵⁶, A. Lusiani²⁴, X. Lyu⁶², F. Machefert⁷, F. Maciuc³⁰, O. Maev³¹, K. Maguire⁵⁵, S. Malde⁵⁶, A. Malinin⁶⁶, T. Maltsev³⁵, G. Manca⁷, G. Mancinelli⁶, P. Manning⁶⁰, J. Maratas^{5,v}, J.F. Marchand⁴, U. Marconi¹⁵, C. Marin Benito³⁷, P. Marino^{24,t}, J. Marks¹², G. Martellotti²⁶, M. Martin⁶, M. Martinelli⁴⁰, D. Martinez Santos³⁸, F. Martinez Vidal⁶⁸, D. Martins Tostes², L.M. Massacrier⁷, A. Massafferri¹, R. Matev³⁹, A. Mathad⁴⁹, Z. Mathe³⁹, C. Matteuzzi²¹, A. Mauri⁴¹, B. Maurin⁴⁰, A. Mazurov⁴⁶, M. McCann⁵⁴, J. McCarthy⁴⁶, A. McNab⁵⁵, R. McNulty¹³, B. Meadows⁵⁸, F. Meier¹⁰, M. Meissner¹², D. Melnychuk²⁹, M. Merk⁴², A. Merli^{22,q}, E. Michielin²³, D.A. Milanes⁶⁴, M.-N. Minard⁴, D.S. Mitzel¹², J. Molina Rodriguez⁶¹, I.A. Monroy⁶⁴, S. Monteil⁵, M. Morandin²³, P. Morawski²⁸, A. Mordà⁶, M.J. Morello^{24,t}, J. Moron²⁸, A.B. Morris⁵¹, R. Mountain⁶⁰, F. Muheim⁵¹, M. Mulder⁴², M. Mussini¹⁵, D. Müller⁵⁵, J. Müller¹⁰, K. Müller⁴¹, V. Müller¹⁰, P. Naik⁴⁷, T. Nakada⁴⁰, R. Nandakumar⁵⁰, A. Nandi⁵⁶, I. Nasteva², M. Needham⁵¹, N. Neri²², S. Neubert¹², N. Neufeld³⁹, M. Neuner¹², A.D. Nguyen⁴⁰, C. Nguyen-Mau^{40,n}, S. Nieswand⁹, R. Niet¹⁰, N. Nikitin³³, T. Nikodem¹², A. Novoselov³⁶, D.P. O'Hanlon⁴⁹, A. Oblakowska-Mucha²⁸, V. Obraztsov³⁶, S. Ogilvy¹⁹, R. Oldeman⁴⁸, C.J.G. Onderwater⁶⁹, J.M. Otalora Goicochea², A. Otto³⁹, P. Owen⁴¹, A. Oyanguren⁶⁸, P.R. Pais⁴⁰, A. Palano^{14,d}, F. Palombo^{22,q}, M. Palutan¹⁹, J. Panman³⁹, A. Papanestis⁵⁰, M. Pappagallo⁵², L.L. Pappalardo^{17,g}, C. Pappenheimer⁵⁸, W. Parker⁵⁹, C. Parkes⁵⁵, G. Passaleva¹⁸, G.D. Patel⁵³, M. Patel⁵⁴, C. Patrignani^{15,*e}, A. Pearce^{55,50}, A. Pellegrino⁴², G. Penso^{26,k}, M. Pepe Altarelli³⁹, S. Perazzini³⁹, P. Perret⁵, L. Pescatore⁴⁶, K. Petridis⁴⁷, A. Petrolini^{20,h}, A. Petrov⁶⁶, M. Petruzzo^{22,q}, E. Picatoste Olloqui³⁷, B. Pietrzyk⁴, M. Pikiés²⁷, D. Pinci²⁶, A. Pistone²⁰, A. Piucci¹², S. Playfer⁵¹, M. Plo Casasus³⁸, T. Poikela³⁹, F. Polci⁸, A. Poluektov^{49,35}, I. Polyakov⁶⁰, E. Polcarpo², G.J. Pomery⁴⁷, A. Popov³⁶, D. Popov^{11,39}, B. Popovici³⁰, C. Potterat², E. Price⁴⁷, J.D. Price⁵³, J. Prisciandaro³⁸, A. Pritchard⁵³, C. Prouve⁴⁷, V. Pugatch⁴⁵, A. Puig Navarro⁴⁰, G. Punzi^{24,p}, W. Qian⁵⁶, R. Quagliani^{7,47}, B. Rachwal²⁷, J.H. Rademacker⁴⁷, M. Rama²⁴, M. Ramos Pernas³⁸, M.S. Rangel², I. Raniuk⁴⁴, G. Raven⁴³, F. Redi⁵⁴, S. Reichert¹⁰, A.C. dos Reis¹, C. Remon Alepuz⁶⁸, V. Renaudin⁷, S. Ricciardi⁵⁰, S. Richards⁴⁷, M. Rihl³⁹, K. Rinnert^{53,39}, V. Rives Molina³⁷, P. Robbe^{7,39}, A.B. Rodrigues¹, E. Rodrigues⁵⁸, J.A. Rodriguez Lopez⁶⁴, P. Rodriguez Perez⁵⁵, A. Rogozhnikov⁶⁷, S. Roiser³⁹, V. Romanovskiy³⁶, A. Romero Vidal³⁸, J.W. Ronayne¹³, M. Rotondo²³, M.S. Rudolph⁶⁰, T. Ruf³⁹, P. Ruiz Valls⁶⁸, J.J. Saborido Silva³⁸, E. Sadykhov³², N. Sagidova³¹, B. Saitta^{16,f}, V. Salustino Guimaraes², C. Sanchez Mayordomo⁶⁸, B. Sanmartin Sedes³⁸, R. Santacesaria²⁶, C. Santamarina Rios³⁸, M. Santimaria¹⁹, E. Santovetti^{25,j}, A. Sarti^{19,k}, C. Satriano^{26,s}, A. Satta²⁵, D.M. Saunders⁴⁷, D. Savrina^{32,33}, S. Schael⁹, M. Schellenberg¹⁰, M. Schiller³⁹, H. Schindler³⁹, M. Schlupp¹⁰, M. Schmelling¹¹, T. Schmelzer¹⁰, B. Schmidt³⁹, O. Schneider⁴⁰, A. Schopper³⁹, K. Schubert¹⁰, M. Schubiger⁴⁰, M.-H. Schune⁷, R. Schwemmer³⁹, B. Sciascia¹⁹, A. Sciubba^{26,k}, A. Semennikov³², A. Sergi⁴⁶, N. Serra⁴¹, J. Serrano⁶, L. Sestini²³, P. Seyfert²¹, M. Shapkin³⁶, I. Shapoval^{17,44,g}, Y. Shcheglov³¹, T. Shears⁵³, L. Shekhtman³⁵, V. Shevchenko⁶⁶, A. Shires¹⁰, B.G. Siddi¹⁷, R. Silva Coutinho⁴¹, L. Silva de Oliveira², G. Simi^{23,0}, M. Sirendi⁴⁸, N. Skidmore⁴⁷, T. Skwarnicki⁶⁰, E. Smith⁵⁴, I.T. Smith⁵¹, J. Smith⁴⁸, M. Smith⁵⁵, H. Snoek⁴², M.D. Sokoloff⁵⁸, F.J.P. Soler⁵², D. Souza⁴⁷, B. Souza De Paula², B. Spaan¹⁰, P. Spradlin⁵², S. Sridharan³⁹, F. Stagni³⁹, M. Stahl¹², S. Stahl³⁹, P. Stefko⁴⁰, S. Stefkova⁵⁴, O. Steinkamp⁴¹, S. Stemmle¹², O. Stenyakin³⁶, S. Stevenson⁵⁶, S. Stoica³⁰, S. Stone⁶⁰, B. Storaci⁴¹, S. Stracka^{24,t}, M. Straticiuc³⁰, U. Straumann⁴¹, L. Sun⁵⁸, W. Sutcliffe⁵⁴, K. Swientek²⁸, V. Syropoulos⁴³, M. Szczekowski²⁹, T. Szumlak²⁸, S. T'Jampens⁴, A. Tayduganov⁶, T. Tekampe¹⁰, G. Tellarini^{17,g}, F. Teubert³⁹, C. Thomas⁵⁶, E. Thomas³⁹, J. van Tilburg⁴², V. Tisserand⁴, M. Tobin⁴⁰, S. Tolk⁴⁸, L. Tomassetti^{17,g}, D. Tonelli³⁹, S. Topp-Joergensen⁵⁶, F. Toriello⁶⁰, E. Tournefier⁴, S. Tourneur⁴⁰, K. Trabelsi⁴⁰, M. Traill⁵², M.T. Tran⁴⁰, M. Tresch⁴¹, A. Trisovic³⁹, A. Tsaregorodtsev⁶, P. Tsopelas⁴², A. Tully⁴⁸, N. Tuning⁴², A. Ukleja²⁹, A. Ustyuzhanin^{67,66}, U. Uwer¹², C. Vacca^{16,39,f}, V. Vagnoni^{15,39}, S. Valat³⁹, G. Valenti¹⁵, A. Vallier⁷, R. Vazquez Gomez¹⁹, P. Vazquez Regueiro³⁸, S. Vecchi¹⁷, M. van Veghel⁴², J.J. Velthuis⁴⁷, M. Veltri^{18,r}, G. Veneziano⁴⁰, A. Venkateswaran⁶⁰, M. Vernet⁵, M. Vesterinen¹², B. Viaud⁷, D. Vieira¹, M. Vieites Diaz³⁸, X. Vilasis-Cardona^{37,m}, V. Volkov³³, A. Vollhardt⁴¹, B. Voneki³⁹, D. Voong⁴⁷, A. Vorobyev³¹,

V. Vorobyev³⁵, C. Voß⁶⁵, J.A. de Vries⁴², C. Vázquez Sierra³⁸, R. Waldi⁶⁵, C. Wallace⁴⁹, R. Wallace¹³, J. Walsh²⁴, J. Wang⁶⁰, D.R. Ward⁴⁸, H.M. Wark⁵³, N.K. Watson⁴⁶, D. Websdale⁵⁴, A. Weiden⁴¹, M. Whitehead³⁹, J. Wicht⁴⁹, G. Wilkinson^{56,39}, M. Wilkinson⁶⁰, M. Williams³⁹, M.P. Williams⁴⁶, M. Williams⁵⁷, T. Williams⁴⁶, F.F. Wilson⁵⁰, J. Wimberley⁵⁹, M. Winn⁴, J. Wishahi¹⁰, W. Wislicki²⁹, M. Witek²⁷, G. Wormser⁷, S.A. Wotton⁴⁸, K. Wraight⁵², S. Wright⁴⁸, K. Wyllie³⁹, Y. Xie⁶³, Z. Xing⁶⁰, Z. Xu⁴⁰, Z. Yang³, H. Yin⁶³, J. Yu⁶³, X. Yuan³⁵, O. Yushchenko³⁶, M. Zangoli¹⁵, K.A. Zarebski⁴⁶, M. Zavertyaev^{11,c}, L. Zhang³, Y. Zhang⁷, Y. Zhang⁶², A. Zhelezov¹², Y. Zheng⁶², A. Zhokhov³², V. Zhukov⁹, S. Zucchelli¹⁵

¹ Centro Brasileiro de Pesquisas Físicas (CBPF), Rio de Janeiro, Brazil

² Universidade Federal do Rio de Janeiro (UFRJ), Rio de Janeiro, Brazil

³ Center for High Energy Physics, Tsinghua University, Beijing, China

⁴ LAPP, Université Savoie Mont-Blanc, CNRS/IN2P3, Annecy-Le-Vieux, France

⁵ Clermont Université, Université Blaise Pascal, CNRS/IN2P3, LPC, Clermont-Ferrand, France

⁶ CPPM, Aix-Marseille Université, CNRS/IN2P3, Marseille, France

⁷ LAL, Université Paris-Sud, CNRS/IN2P3, Orsay, France

⁸ LPNHE, Université Pierre et Marie Curie, Université Paris Diderot, CNRS/IN2P3, Paris, France

⁹ I. Physikalisches Institut, RWTH Aachen University, Aachen, Germany

¹⁰ Fakultät Physik, Technische Universität Dortmund, Dortmund, Germany

¹¹ Max-Planck-Institut für Kernphysik (MPIK), Heidelberg, Germany

¹² Physikalisches Institut, Ruprecht-Karls-Universität Heidelberg, Heidelberg, Germany

¹³ School of Physics, University College Dublin, Dublin, Ireland

¹⁴ Sezione INFN di Bari, Bari, Italy

¹⁵ Sezione INFN di Bologna, Bologna, Italy

¹⁶ Sezione INFN di Cagliari, Cagliari, Italy

¹⁷ Sezione INFN di Ferrara, Ferrara, Italy

¹⁸ Sezione INFN di Firenze, Firenze, Italy

¹⁹ Laboratori Nazionali dell'INFN di Frascati, Frascati, Italy

²⁰ Sezione INFN di Genova, Genova, Italy

²¹ Sezione INFN di Milano Bicocca, Milano, Italy

²² Sezione INFN di Milano, Milano, Italy

²³ Sezione INFN di Padova, Padova, Italy

²⁴ Sezione INFN di Pisa, Pisa, Italy

²⁵ Sezione INFN di Roma Tor Vergata, Roma, Italy

²⁶ Sezione INFN di Roma La Sapienza, Roma, Italy

²⁷ Henryk Niewodniczański Institute of Nuclear Physics Polish Academy of Sciences, Kraków, Poland

²⁸ AGH – University of Science and Technology, Faculty of Physics and Applied Computer Science, Kraków, Poland

²⁹ National Center for Nuclear Research (NCBJ), Warsaw, Poland

³⁰ Horia Hulubei National Institute of Physics and Nuclear Engineering, Bucharest-Magurele, Romania

³¹ Petersburg Nuclear Physics Institute (PNPI), Gatchina, Russia

³² Institute of Theoretical and Experimental Physics (ITEP), Moscow, Russia

³³ Institute of Nuclear Physics, Moscow State University (SINP MSU), Moscow, Russia

³⁴ Institute for Nuclear Research of the Russian Academy of Sciences (INR RAN), Moscow, Russia

³⁵ Budker Institute of Nuclear Physics (SB RAS) and Novosibirsk State University, Novosibirsk, Russia

³⁶ Institute for High Energy Physics (IHEP), Protvino, Russia

³⁷ ICCUB, Universitat de Barcelona, Barcelona, Spain

³⁸ Universidad de Santiago de Compostela, Santiago de Compostela, Spain

³⁹ European Organization for Nuclear Research (CERN), Geneva, Switzerland

⁴⁰ Ecole Polytechnique Fédérale de Lausanne (EPFL), Lausanne, Switzerland

⁴¹ Physik-Institut, Universität Zürich, Zürich, Switzerland

⁴² Nikhef National Institute for Subatomic Physics, Amsterdam, The Netherlands

⁴³ Nikhef National Institute for Subatomic Physics and VU University Amsterdam, Amsterdam, The Netherlands

⁴⁴ NSC Kharkiv Institute of Physics and Technology (NSC KIPT), Kharkiv, Ukraine

⁴⁵ Institute for Nuclear Research of the National Academy of Sciences (KINR), Kyiv, Ukraine

⁴⁶ University of Birmingham, Birmingham, United Kingdom

⁴⁷ H.H. Wills Physics Laboratory, University of Bristol, Bristol, United Kingdom

⁴⁸ Cavendish Laboratory, University of Cambridge, Cambridge, United Kingdom

⁴⁹ Department of Physics, University of Warwick, Coventry, United Kingdom

⁵⁰ STFC Rutherford Appleton Laboratory, Didcot, United Kingdom

⁵¹ School of Physics and Astronomy, University of Edinburgh, Edinburgh, United Kingdom

⁵² School of Physics and Astronomy, University of Glasgow, Glasgow, United Kingdom

⁵³ Oliver Lodge Laboratory, University of Liverpool, Liverpool, United Kingdom

⁵⁴ Imperial College London, London, United Kingdom

⁵⁵ School of Physics and Astronomy, University of Manchester, Manchester, United Kingdom

⁵⁶ Department of Physics, University of Oxford, Oxford, United Kingdom

⁵⁷ Massachusetts Institute of Technology, Cambridge, MA, United States

⁵⁸ University of Cincinnati, Cincinnati, OH, United States

⁵⁹ University of Maryland, College Park, MD, United States

⁶⁰ Syracuse University, Syracuse, NY, United States

⁶¹ Pontifícia Universidade Católica do Rio de Janeiro (PUC-Rio), Rio de Janeiro, Brazil^w

⁶² University of Chinese Academy of Sciences, Beijing, China^x

⁶³ Institute of Particle Physics, Central China Normal University, Wuhan, Hubei, China^x

⁶⁴ Departamento de Física, Universidad Nacional de Colombia, Bogotá, Colombia^y

⁶⁵ Institut für Physik, Universität Rostock, Rostock, Germany^z

⁶⁶ National Research Centre Kurchatov Institute, Moscow, Russia^{aa}

⁶⁷ Yandex School of Data Analysis, Moscow, Russia ^{aa}

⁶⁸ Instituto de Física Corpuscular (IFIC), Universitat de Valencia-CSIC, Valencia, Spain ^{ab}

⁶⁹ Van Swinderen Institute, University of Groningen, Groningen, The Netherlands ^{ac}

* Corresponding authors.

E-mail addresses: roberta.cardinale@cern.ch (R. Cardinale), claudia.patrignani@cern.ch (C. Patrignani).

^a Universidade Federal do Triângulo Mineiro (UFMT), Uberaba-MG, Brazil.

^b Laboratoire Leprince-Ringuet, Palaiseau, France.

^c P.N. Lebedev Physical Institute, Russian Academy of Science (LPI RAS), Moscow, Russia.

^d Università di Bari, Bari, Italy.

^e Università di Bologna, Bologna, Italy.

^f Università di Cagliari, Cagliari, Italy.

^g Università di Ferrara, Ferrara, Italy.

^h Università di Genova, Genova, Italy.

ⁱ Università di Milano Bicocca, Milano, Italy.

^j Università di Roma Tor Vergata, Roma, Italy.

^k Università di Roma La Sapienza, Roma, Italy.

^l AGH – University of Science and Technology, Faculty of Computer Science, Electronics and Telecommunications, Kraków, Poland.

^m LIFAELS, La Salle, Universitat Ramon Llull, Barcelona, Spain.

ⁿ Hanoi University of Science, Hanoi, Viet Nam.

^o Università di Padova, Padova, Italy.

^p Università di Pisa, Pisa, Italy.

^q Università degli Studi di Milano, Milano, Italy.

^r Università di Urbino, Urbino, Italy.

^s Università della Basilicata, Potenza, Italy.

^t Scuola Normale Superiore, Pisa, Italy.

^u Università di Modena e Reggio Emilia, Modena, Italy.

^v Iligan Institute of Technology (IIT), Iligan, Philippines.

^w Associated to Universidade Federal do Rio de Janeiro (UFRJ), Rio de Janeiro, Brazil.

^x Associated to Center for High Energy Physics, Tsinghua University, Beijing, China.

^y Associated to LPNHE, Université Pierre et Marie Curie, Université Paris Diderot, CNRS/IN2P3, Paris, France.

^z Associated to Physikalisches Institut, Ruprecht-Karls-Universität Heidelberg, Heidelberg, Germany.

^{aa} Associated to Institute of Theoretical and Experimental Physics (ITEP), Moscow, Russia.

^{ab} Associated to ICCUB, Universitat de Barcelona, Barcelona, Spain.

^{ac} Associated to Nikhef National Institute for Subatomic Physics, Amsterdam, The Netherlands.